2024 IEEE International Conference on Robotics and Automation (ICRA 2024)
May 13-17, 2024. Yokohama, Japan

Hydrodynamic Interactions in Schooling Fish: Prioritizing Real Fish Kinematics Over Travelling-wavy Undulation

Li-Ming Chao [1,2,3] and Liang Li [1,2,3]

Abstract— **Hydrodynamic interactions are crucial for understanding fish movement, particularly within the realm of robotic applications. Traditionally, many studies have favoured simplified travelling-wavy undulations derived from observed real fish kinematics. This approach often neglects higher-order undulations, thereby missing the subtleties of authentic fish movements. In this study, we utilised Computational Fluid Dynamics (CFD) to investigate the implications of using real fish kinematics in hydrodynamic interactions among schooling fish. We analysed two scenarios: one driven by real fish kinematics in spatiotemporal formations, and the other by travelling-wavy undulations inferred from the same real fish kinematics. Our results highlight the advantages of using real fish body kinematics for a more accurate representation of hydrodynamics in fish swimming. In contrast, the idealised travelling-wavy undulations tend to apply excessive force, displacing real fish more than expected. Additionally, the vortices and corresponding flow fields generated by real fish kinematics were found to be more stable than those arising from simplified travelling-wavy undulations. Our study underscores the significance of integrating real fish kinematics into robotic fish design and hydrodynamic studies in schooling fish.**

I. INTRODUCTION

After almost half a billion years of evolution, fish have evolved highly effective swimming abilities in complex underwater environments [1]. This has drawn considerable attention in multiple disciplines, including biology, engineering, physics, and mathematics [2], [3]. For example, previous studies have demonstrated that fish could improve swimming efficiency via a suite of adaptations, including refinement of the surface structures to reduce drag [4], adjusting the flexibility of the tail [5], and optimizing swimming kinematics [6]–[8].

Recently, there has been a growing interest in understanding whether individuals living in groups can extract energy from the vortices shed by their neighbours to enhance their collective swimming efficiency [9]–[14]. However, most studies in this domain have postulated that fish swim using idealised travelling-wavy undulations, which may or may not be based on actual fish movement data [6], [15]. Although some research has also applied reinforcement learning, they have to assume that all fish are pursuing a uniformly defined reward and employ reinforcement learning techniques to optimise their swimming actions accordingly [9].

Estimating hydrodynamic interactions in real fish swimming is extremely challenging [16], especially when the behaviour of interest occurs occasionally. However, thanks to advancements in computer vision and computational capabilities, we can now capture 2D and/or 3D patterns of fish swimming [17] and conduct simulations to delve into the intricate hydrodynamics between simulated fish bodies [14], [18]. In this paper, our objective is to quantitatively evaluate the importance of integrating real fish kinematics into computational models, in comparison to the traditional travelling-wavy undulations derived from the same real fish kinematics (Fig. 1). To accomplish this, we monitored real fish swimming in a flow tank, captured their real kinematics, formulated idealised travelling-wavy undulations based on these kinematics [8], [19] (Fig. 1, Biology), and then conducted computational fluid simulations using both the real fish kinematics and the modelled travelling-wavy undulations (Fig. 1, Physics). Our analysis compared the resultant forces from these two swimming modes and linked them with fish movements observed in natural settings. We found that simulations grounded in real fish kinematics yield more accurate force data and exhibit greater stability through the lens of vortices, compared to those based on idealised travelling-wavy undulations. This suggests that the real kinematics of real fish should be considered in hydrodynamic studies, offering potential applications for future robotics. (Fig. 1, Engineering).

II. FISH EXPERIMENTS AND TRAVELLING-WAVY UNDULATION MODELLING

A. Experiments with real fish system

We conducted experiments in a flow tank from Loligo Systems (Tjele, Denmark) at the Max Planck Institute of Animal Behavior, located in Konstanz, Germany. The flow tank's effective testing area measures 0.25 m in width, 0.875 m in length, and 0.25 m in depth. A mirror was positioned beneath the tank at a 45-degree angle, enabling the capture of the bottom view. We utilised BASLER acA2000-165umNIR cameras to record fish movements from both bottom and lateral perspectives at a rate of 100 frames per second and a resolution of 2048×1058. The video recording was facilitated by a specialised setup from Loopbio, Austria.

Building on our prior research [10], we selected goldfish (*Carassius auratus*) measuring between 15-20 cm in body size to enhance the likelihood of hydrodynamic interactions,

*This work was supported by the Max-Planck Society, the Deutsche Forschungsgemeinschaft (DFG, German Research Foundation) under Germany's Excellence Strategy–EXC 2117-422037984, the Sino-German Centre in Beijing for generous funding of the Sino-German mobility grant M-0541, and Messmer Foundation Research Award.

[1] Department of Collective Behaviour, Max Planck Institute of Animal Behavior, Konstanz, Germany
[2] Centre for the Advanced Study of Collective Behaviour, University of Konstanz, Konstanz, Germany
[3] Department of Biology, University of Konstanz, Konstanz, Germany
lli@ab.mpg.de, liang.li@uni-konstanz.de

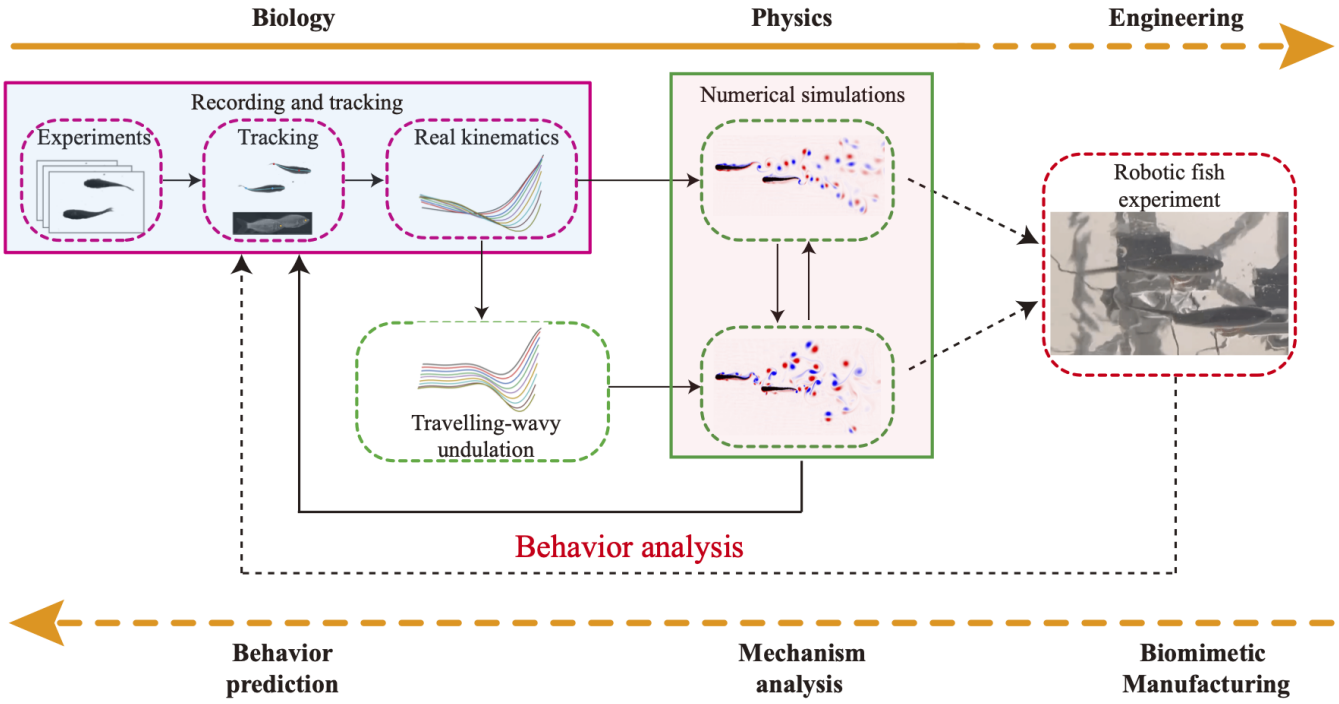

Fig. 1: Schematic overview of research schedule and future prospects. The solid line (Biology and Physics) denotes the work performed in present studies, while the dashed lines (Engineering) refer to our future investigations.

while ensuring ample room for schooling within our flow tank (Fig. 2). We adjusted the flow speed to range from 1.2 to 1.6 body lengths per second (BL/s), with increments of 0.1 BL/s, aligning with their typical cruising speeds [20]. Before initiating the experiments, the fish were allowed to acclimate to the flow tank for 30 minutes. For the experiments conducted here, we randomly selected the flow speed and collected fish schooling at that flow speed for approximately 5 minutes. Following each recording, the fish were given a rest period of at least 5 minutes. This process was carried out over a span of 3 hours. All experimental procedures received approval from Regierungspräsidium Freiburg (35-9185.81/G-17/90).

Tracking was executed in both bottom and side views using deep learning algorithms [21], [22]. Initially, DeepLabCut [21] was employed to identify the nose and left eye of each fish from the bottom-view and side-view videos, respectively. Leveraging the detected nose positions, we integrated a Kalman filter and Hungarian algorithm for fish tracking. With the tracked positions as a foundation, we isolated each fish and undertook posture tracking using the DeepPoseKit software [22]. Consequently, we quantified the movements and kinematics of the fish's center line, utilizing these spatiotemporal attributes to characterize the genuine kinematics of the fish in our experiments. More details on how we obtained the spatiotemporal movements and postures of swimming fish can be found in [17].

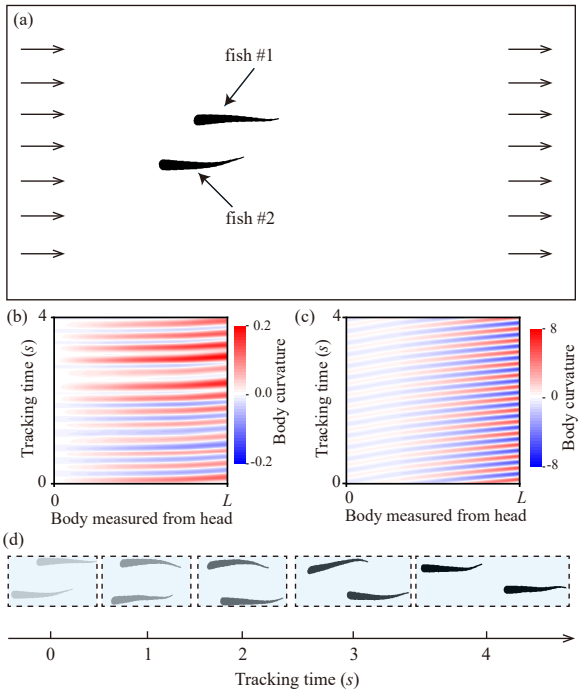

Fig. 2: Fish body kinematics analyses. (a) Sketch of the experiments with real fish. (b-c) Body curvature of fish #1 for (b) real kinematics (RK) and (c) travelling-wavy undulation (TU). (d) Spatiotemporal evolution of numerical fish swimming in RK mode.

B. Travelling-wavy undulation modeling

The travelling-wavy undulation is commonly utilised to characterize the rhythmic movement of the fish body, which often involves two parts. One part pertains to the cyclic

curvature changes of the fish's body, resulting in the lateral propagation of waves towards the tail. The other part manifests as each point along the body following a sinusoidal trajectory within a horizontal plane due to the wave propagation [23]. Through travelling-wavy undulation, the fish effectively transports fluid mass from its anterior to posterior regions. This fluid mass transport mechanism can be interpreted as the local momentum transfer in the streamwise direction, which plays a pivotal role in generating thrust. For further elucidation on the intricacies of travelling-wavy undulation, comprehensive discussions are available in [15].

We simplified fish locomotion into a travelling-wavy undulation (TU) based on the spatiotemporal properties of each fish. We model the TU as follows:

$$y_i(x_i,t) = Y_i(t) + A(x_i)\sin\left[2\pi(\frac{x_i}{\lambda_i} - f_i t)\right], \qquad (1)$$

where the subscript i (=1, 2) identifies fish #1 (upper one, Fig. 2) and fish #2 (bottom one, Fig. 2), $A(x)$ represents the swimming amplitude function, typically expressed as a polynomial function $A(x) = a + bx + cx^2$ [19], [24], y is the lateral displacement of fish, x is measured from the fish head, Y is the lateral location of the fish head from the tracking results, λ is the wavelength, f is the undulating frequency, and t is the instantaneous time. Note all distances in the present work are normalised by fish length L.

Using the dataset derived from fish experiments (x, y, t), we first estimated the frequency f_i in Eq. 1 via the Fast Fourier Transform (FFT) method. As illustrated in Fig. 3, the values $f_1 = 3.580$ Hz and $f_2 = 4.568$ Hz, which represent the highest magnitudes, correspond to the primary frequencies adopted by fish #1 and fish #2, respectively. We then applied the kernel density estimate (KDE) method to determine the values of λ, a, b, and c (see Fig. 3). Thus, based on spatiotemporal properties, the travelling-wavy undulations (TUs) can be summarised as follows:

$$\begin{aligned} y_1(x_1,t) =& Y_1(t) + (0.135 - 0.048x + 0.002x^2) \\ & \cdot \sin\left[2\pi(\frac{x_1}{0.795} - 3.580t)\right], \qquad \text{fish \#1}, \\ y_2(x_2,t) =& Y_2(t) + (-0.094 + 0.060x - 0.003x^2) \\ & \cdot \sin\left[2\pi(\frac{x_2}{0.753} - 4.568t)\right], \qquad \text{fish \#2}. \end{aligned} \qquad (2)$$

In Figs. 2(b) and (c), the body curvatures of fish #1 are illustrated for the real kinematics (RK) and TU modes, respectively. We observed that fish swimming in the RK mode exhibit more irregular changes in body curvature compared to those swimming in the TU mode. Furthermore, it's noteworthy that the curvature values produced by RK are significantly lower than those generated by TU. This difference can be ascribed to the intrinsic structural limitations of real fish.

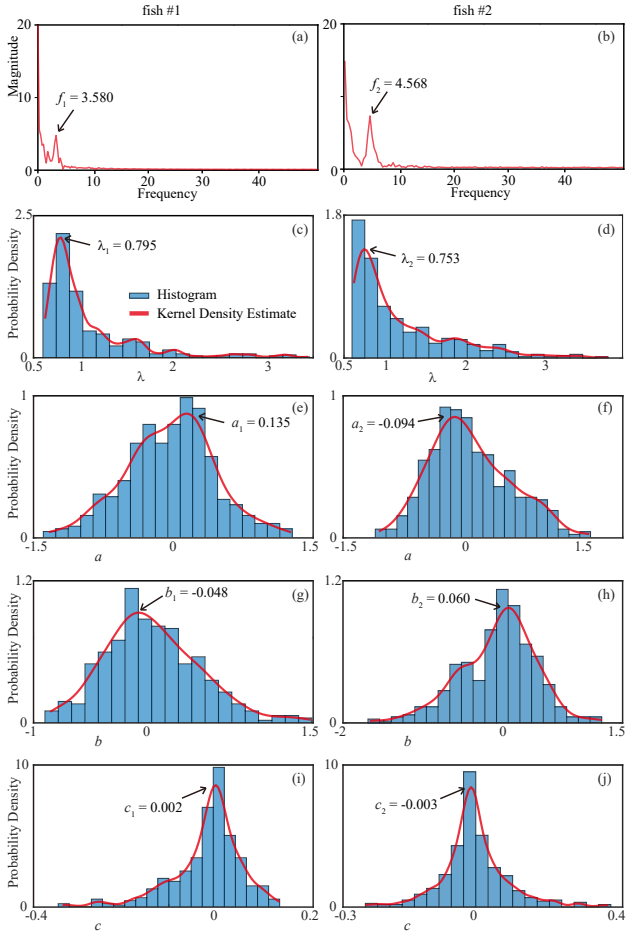

Fig. 3: Determining parameters for the TU mode model. (a-b) Frequency determination for fish #1 and fish #2. (c-d) Determination of body wavelength. (e-j) Coefficient determination for a_i (e-f), b_i (g-h), and c_i (i-j).

III. Computational Fluid Dynamics Simulations and Results

A. Computational fluid dynamics simulations

The unsteady flow field around two fish was simulated using the immersed boundary (IB) method. The IB formulation of fluid–structure interaction (FSI) uses an Eulerian description of the fluid and a Lagrangian description of the structure. Interaction equations that couple the Eulerian and Lagrangian variables take the form of integral equations with delta function kernels [25], [26].

In our research, two fish are compelled to move with identical spatiotemporal formations (with the prescribed velocity $\mathbf{V}(\mathbf{s}, t)$), yet they exhibit different body kinematics: one mimics the movement of real fish, while the other follows the extracted travelling-wavy undulation (Eq. 2). Referring [27], the associated IB formulations are as follows:

$$\rho\frac{\mathrm{D}\mathbf{u}}{\mathrm{D}t}(\mathbf{x},t) = -\nabla p(\mathbf{x},t) + \mu\nabla^2\mathbf{u}(\mathbf{x},t) + \mathbf{f}(\mathbf{x},t), \qquad (3)$$

$$\nabla\cdot\mathbf{u}(\mathbf{x},t) = 0, \qquad (4)$$

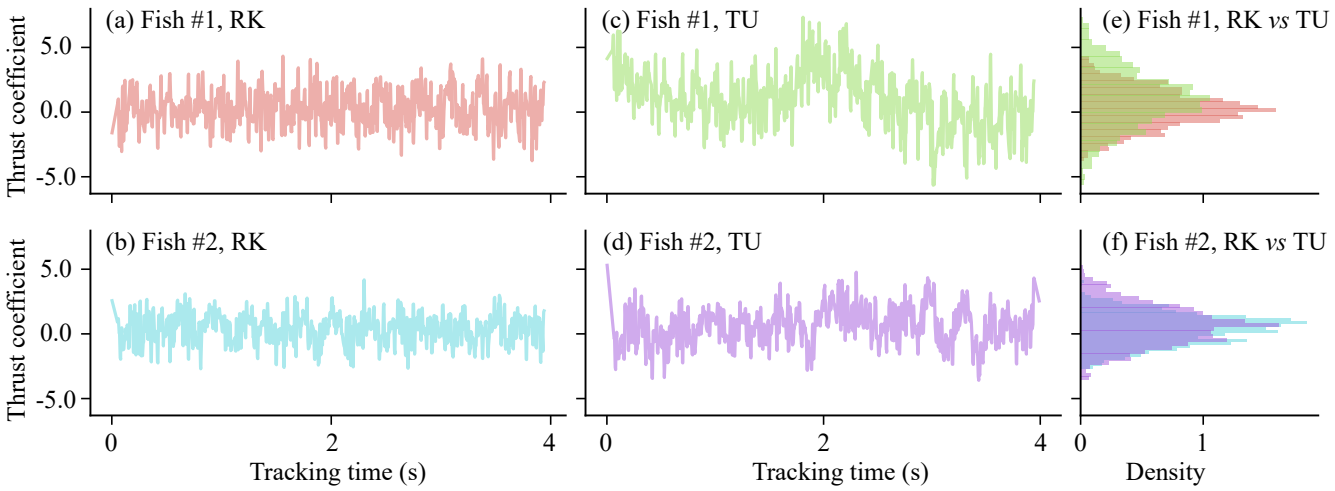

Fig. 4: Swimming performance analyses of numerical schooling fish swimming in RK and TU modes. (a-d) The thrust coefficient for two numerical fish in two swimming modes. (e,f) Statistic results of thrust coefficient generated by (e) fish #1 and (f) fish #2, respectively.

$$\mathbf{U}(\mathbf{s},t) = \int_{\Omega} \mathbf{u}(\mathbf{x},t)\delta\left[\mathbf{x} - \chi(\mathbf{s},t)\right] \mathrm{d}\mathbf{x}, \tag{5}$$

$$\mathbf{U}(\mathbf{s},t) = \mathbf{V}(\mathbf{s},t), \tag{6}$$

$$\frac{\partial \chi}{\partial t}(\mathbf{s},t) = \mathbf{V}(\mathbf{s},t), \tag{7}$$

$$\mathbf{f}(\mathbf{x},t) = \int_{\Omega_c} F(\mathbf{s},t)\delta\left[\mathbf{x} - \chi(\mathbf{s},t)\right] \mathrm{d}\mathbf{x}, \tag{8}$$

where ρ represents the fluid density, $\mathrm{D}/\mathrm{D}t = \partial/\partial t + \mathbf{u}(\mathbf{x},t) \cdot \nabla$ is the convective derivative, $\mathbf{u}(\mathbf{x},t)$ denotes the fluid velocity described in Eulerian form, $\mathbf{x}$ is physical coordinates, $p(\mathbf{x},t)$ is the static pressure, μ is the viscosity of the fluid, $\mathbf{f}(\mathbf{x},t)$ is the body force that acts to enforce the constraints imposed on the parts of the body, $\mathbf{U}(\mathbf{s},t)$ is the Lagrangian velocity of the body, $\chi(\mathbf{s},t)$ is the physical position of material point s at time t, δ is the Dirac delta function, Ω is the physical space, and Ω_c is the parts of the body where constraints are imposed on the body motion.

We carried out numerical analyses using the open-source IBAMR (Immersed Boundary Method Adaptive Mesh Refinement) software. This tool offers a distributed-memory parallel implementation of the immersed boundary (IB) method, integrating the Cartesian grid adaptive mesh refinement (AMR) technique [27]. The IBAMR software has been widely employed in studies of fish-like swimming [18], [28]–[30]. The computational domain is defined as a rectangular box, mirroring the boundary conditions of the flow tank utilised in our fish experiments (see Fig. 2a). This includes an inlet velocity boundary on the left side with a consistent flow speed, no-stress outflow boundary conditions on the right, and no-slip wall conditions for both the top and bottom boundaries.

The simulated fish geometry closely resembles that of typical *carangiform* swimmers, a classification known for its characteristic features, including:

$$w(x) = \begin{cases} \sqrt{2W_H x - x^2} & 0 \le x < x_H \\ W_H \frac{1-x}{1-x_H} & x_H \le x \le 1, \end{cases} \tag{9}$$

where $w(x)$ is fish's width at x, and $W_H = x_H = 0.12$. As our primary focus is on the function of body kinematics in hydrodynamic interactions, we assume that numerical fish share identical body shapes, although these may vary slightly from those in real fish systems. Figure 2(d) illustrates the spatiotemporal evolution of numerical fish in RK mode.

B. Results

We collected the propulsive force (thrust) coefficient data for two numerical fish in two different swimming modes: RK, which represents movement with real fish kinematics, and TU, which represents movement with travelling-wavy undulation. To ensure that the two numerical fish maintained the same spatiotemporal formations as the real fish, thus allowing us to replicate similar hydrodynamic interactions, we enforced the positions of the two fish to mimic those observed in the real fish system. Figure 4 (a-d) depicts propulsive force and power coefficient [18] data for two numerical fish in distinct swimming modes. Due to our use of traction boundary conditions, the original data directly obtained from numerical simulations exhibit instabilities [31]. However, we still clearly see that fish achieve greater thrust stability with RK mode, compared to fish swimming in TU mode. These fluctuations in TU mode indicate a pronounced fluid-structure interaction around the fish, highlighting the substantial impact of the fluid on fish locomotion, which may potentially impair its swimming performance.

We further analysed the median of the simulated thrust coefficient for fish swimming in both the RK and TU modes. A value closer to 0 indicates that our simulations more

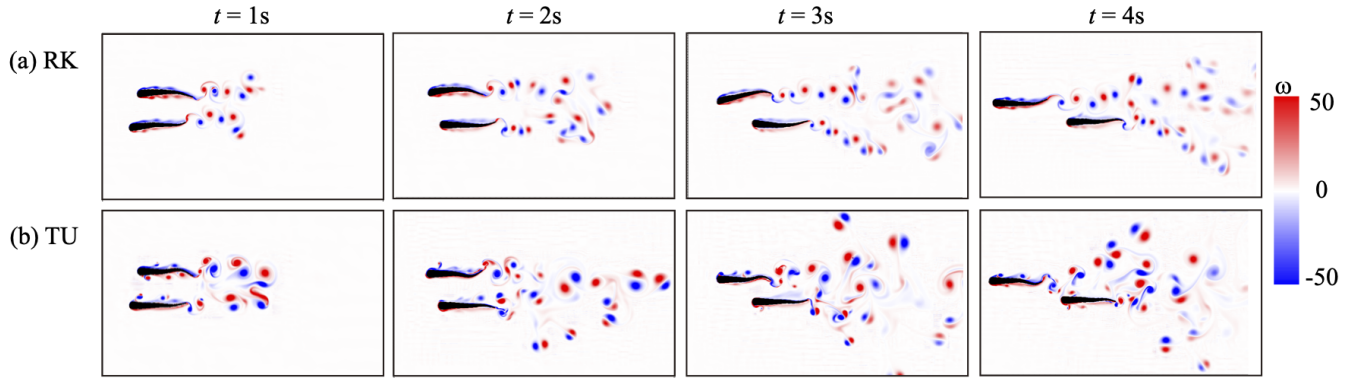

Fig. 5: Vortex structures of two numerical schooling fish in (a) real kinematics (RK) and (b) travelling-wavy undulation (TU) modes. ω is the spanwise vorticity along z-axis.

closely mirror reality, as the numerical fish display average accelerations akin to those of actual self-propelled fish. From our analyses, we found values of 0.036 for fish #1 in RK mode, 0.175 for fish #1 in TU mode, -0.012 for fish #2 in RK mode, and 0.086 for fish #2 in TU mode, as illustrated in Fig. 4 (e and f). Both fish #1 and #2 exhibited values closer to 0 when swimming in RK mode compared to the TU mode. Furthermore, influenced by the incoming flow, Fish #2 displayed rearward motion, suggesting it should generate a negative thrust. This is in contrast to the positive value indicated by the TU mode. These results highlight that the TU mode may not accurately capture the hydrodynamic performance of real swimming fish.

To further understand why the travelling-wavy undulation introduces significant discrepancies in estimating the swimming performance of fish #2, we visualised the flow structures around two schooling fish. Figure 5 shows that the travelling-wavy undulation creates a chaotic wake behind fish #2. In contrast, fish swimming in the RK mode generate slanted reverse Bénard–von Kármán vortex street patterns for fish #2. This outcome again implies that real fish can actively and effectively regulate vortex structures through kinematic adjustments during hydrodynamic interactions with their conspecifics.

IV. Conclusion, Discussion and Outlook

In this study, we examined and compared the swimming performances of two schooling fish, focusing on their hydrodynamic interactions. Using computational fluid dynamics simulations, we modelled fish movements based on real fish kinematics (RK) mode and an idealised travelling-wavy undulation (TU) mode derived from the same motions. The results indicate that fish in the RK mode produce forces closely aligned with their movements, both for the leading and following fish. This suggests that the forces experienced by both fish closely resemble self-propulsion, as observed in actual fish. In contrast, fish swimming in the TU mode display higher biases, diverging significantly from the self-propulsion mode. Flow visualisation revealed that followers in RK mode can actively adapt to leader-generated wake structures and efficiently manage vortex formations. Through vortex analyses, we observed that swimming stability is greater in RK mode compared to TU mode. Our research suggests that the idealised travelling-wavy undulation, even though derived from real fish kinematics, is not a precise method for assessing fish swimming performance, especially in intricate flow conditions such as swimming in the wakes of conspecifics or heterospecifics.

To model the travelling-wavy undulation, we employed a numerical optimization approach to parametrically estimate the trajectories of real fish kinematics, resulting in the 'long-term' average kinematics. However, this would ignore certain active adjustments in the spatiotemporal characteristics of fish kinematics in response to complex flow environments. For example, trout actively adjust their posture in response to the Bénard–von Kármán vortex street to reduce muscle energy consumption [32], while goldfish employ vortex phase matching strategies to harness energy from the flow patterns generated by the leader [10]. Furthermore, we aligned the head position of the numerical fish with real kinematics using prescribed motion control. However, fish employing travelling-wavy undulation may not attain the same positions as real kinematics.

In our investigation of the swimming performance of schooling fish, we predominantly employed two-dimensional simulations grounded in real fish kinematics and travelling-wavy undulation. In the future, we plan to employ other advanced methods for extracting descriptions of body waves and compare these with the actual kinematics of real fish. This will include approaches such as central pattern generators (CPGs) [33] and dynamic movement primitives (DMPs) [34]. It's also crucial to note that fish inhabit a 3D environment, produce 3D fluid dynamics, and experience 3D hydrodynamic interactions. Our recent research leveraged the RoboTwin platform [35], which boasts features such as a flow tank system, recording and tracking functionalities, advanced robotic fish models, a multi-axis position control system, thrust measurement tools, and a particle image velocimetry (PIV) system. Through the combined insights from our CFD and robotic experiments, we can comprehend how fish perceive flow and make corresponding movement decisions. Such understanding will ultimately inspire engi-

neers to design and control man-made vehicles that move more efficiently.

REFERENCES

[1] M. Lighthill, "Hydromechanics of aquatic animal propulsion," *Annual review of fluid mechanics*, vol. 1, no. 1, pp. 413–446, 1969.

[2] M. S. Triantafyllou, G. Triantafyllou, and D. Yue, "Hydrodynamics of fishlike swimming," *Annual review of fluid mechanics*, vol. 32, no. 1, pp. 33–53, 2000.

[3] F. E. Fish and G. V. Lauder, "Passive and active flow control by swimming fishes and mammals," *Annu. Rev. Fluid Mech.*, vol. 38, pp. 193–224, 2006.

[4] L. Wen, J. C. Weaver, and G. V. Lauder, "Biomimetic shark skin: design, fabrication and hydrodynamic function," *Journal of experimental Biology*, vol. 217, no. 10, pp. 1656–1666, 2014.

[5] Q. Zhong, J. Zhu, F. E. Fish, S. J. Kerr, A. Downs, H. Bart-Smith, and D. Quinn, "Tunable stiffness enables fast and efficient swimming in fish-like robots," *Science Robotics*, vol. 6, no. 57, p. eabe4088, 2021.

[6] A. P. Maertens, A. Gao, and M. S. Triantafyllou, "Optimal undulatory swimming for a single fish-like body and for a pair of interacting swimmers," *Journal of Fluid Mechanics*, vol. 813, pp. 301–345, 2017.

[7] L.-M. Chao, M. M. Alam, and C. Ji, "Drag–thrust transition and wake structures of a pitching foil undergoing asymmetric oscillation," *Journal of Fluids and Structures*, vol. 103, p. 103289, 2021.

[8] L. Li, C. Wang, R. Fan, and G. Xie, "Exploring the backward swimming ability of a robotic fish: Combining modelling and experiments," *International Journal of Advanced Robotic Systems*, vol. 13, no. 5, p. 1729881416669483, 2016.

[9] S. Verma, G. Novati, and P. Koumoutsakos, "Efficient collective swimming by harnessing vortices through deep reinforcement learning," *Proceedings of the National academy of Sciences of the United States of America*, vol. 115, no. 23, pp. 5849–5854, 2018.

[10] L. Li, M. Nagy, J. M. Graving, J. Bak-Coleman, G. Xie, and I. D. Couzin, "Vortex phase matching as a strategy for schooling in robots and in fish," *Nature communications*, vol. 11, no. 1, p. 5408, 2020.

[11] L. Li, S. Ravi, G. Xie, and I. D. Couzin, "Using a robotic platform to study the influence of relative tailbeat phase on the energetic costs of side-by-side swimming in fish," *Proceedings of the Royal Society a-Mathematical Physical and Engineering Sciences*, 2021.

[12] D. Weihs, "Hydromechanics of fish schooling," *Nature*, vol. 241, no. 5387, pp. 290–291, 1973.

[13] X. Zhu, G. He, and X. Zhang, "Flow-mediated interactions between two self-propelled flapping filaments in tandem configuration," *Physical Review Letters*, vol. 113, no. 23, p. 238105, 2014.

[14] A. Filella, F. Nadal, C. Sire, E. Kanso, and C. Eloy, "Model of collective fish behavior with hydrodynamic interactions," *Physical review letters*, vol. 120, no. 19, p. 198101, 2018.

[15] L.-M. Chao, M. M. Alam, and L. Cheng, "Hydrodynamic performance of slender swimmer: effect of travelling wavelength," *Journal of Fluid Mechanics*, vol. 947, p. A8, 2022.

[16] B. E. Flammang, G. V. Lauder, D. R. Troolin, and T. E. Strand, "Volumetric imaging of fish locomotion," *Biology Letters*, vol. 7, no. 5, p. 695–698, 2011.

[17] R. Wu, O. Deussen, and L. Li, "Deepshapekit: accurate 4d shape reconstruction of swimming fish," in *2022 IEEE/RSJ International Conference on Intelligent Robots and Systems (IROS)*, pp. 526–531, IEEE, 2022.

[18] L.-M. Chao, A. P. S. Bhalla, and L. Li, "Vortex interactions of two burst-and-coast swimmers in a side-by-side arrangement," *Theoretical and Computational Fluid Dynamics*, pp. 1–13, 2023.

[19] L. Li, C. Wang, and G. Xie, "Modeling of a carangiform-like robotic fish for both forward and backward swimming: Based on the fixed point," May 2014.

[20] R. W. Radcliffe, "The effect of fin–clipping on the cruising speed of goldfish and coho salmon fry," *Journal of the Fisheries Board of Canada*, vol. 8, no. 2, pp. 67–73, 1950.

[21] A. Mathis, P. Mamidanna, K. M. Cury, T. Abe, V. N. Murthy, M. W. Mathis, and M. Bethge, "Deeplabcut: markerless pose estimation of user-defined body parts with deep learning," *Nature neuroscience*, vol. 21, no. 9, p. 1281, 2018.

[22] J. M. Graving, D. Chae, H. Naik, L. Li, B. Koger, B. R. Costelloe, and I. D. Couzin, "Deepposekit, a software toolkit for fast and robust animal pose estimation using deep learning," *eLife*, vol. 8, p. e47994, 2019.

[23] J. Gray, "Studies in animal locomotion: I. the movement of fish with special reference to the eel," *Journal of experimental biology*, vol. 10, no. 1, pp. 88–104, 1933.

[24] D. Barrett, M. Grosenbaugh, and M. Triantafyllou, "The optimal control of a flexible hull robotic undersea vehicle propelled by an oscillating foil," 1996.

[25] C. S. Peskin, "The immersed boundary method," *Acta numerica*, vol. 11, pp. 479–517, 2002.

[26] R. Mittal and G. Iaccarino, "Immersed boundary methods," *Annual review of fluid mechanics*, vol. 37, pp. 239–261, 2005.

[27] B. E. Griffith and N. A. Patankar, "Immersed methods for fluid–structure interaction," *Annual review of fluid mechanics*, vol. 52, pp. 421–448, 2020.

[28] A. P. S. Bhalla, R. Bale, B. E. Griffith, and N. A. Patankar, "A unified mathematical framework and an adaptive numerical method for fluid–structure interaction with rigid, deforming, and elastic bodies," *Journal of Computational Physics*, vol. 250, pp. 446–476, 2013.

[29] A. P. Hoover, R. Cortez, E. D. Tytell, and L. J. Fauci, "Swimming performance, resonance and shape evolution in heaving flexible panels," *Journal of Fluid Mechanics*, vol. 847, pp. 386–416, 2018.

[30] D. Zhang, G. Pan, L. Chao, and Y. Zhang, "Effects of reynolds number and thickness on an undulatory self-propelled foil," *Physics of Fluids*, vol. 30, no. 7, 2018.

[31] M. E. Moghadam, Y. Bazilevs, T.-Y. Hsia, I. E. Vignon-Clementel, and A. L. Marsden, "A comparison of outlet boundary treatments for prevention of backflow divergence with relevance to blood flow simulations," *Computational Mechanics*, vol. 48, no. 3, pp. 277–291, 2011.

[32] J. C. Liao, D. N. Beal, G. V. Lauder, and M. S. Triantafyllou, "Fish exploiting vortices decrease muscle activity," *Science*, vol. 302, no. 5650, pp. 1566–1569, 2003.

[33] L. Li, C. Wang, and G. Xie, "A general cpg network and its implementation on the microcontroller," *Neurocomputing*, vol. 167, pp. 299–305, 2015.

[34] I. Hameed, X. Chao, D. Navarro-Alarcon, and X. Jing, "Training dynamic motion primitives using deep reinforcement learning to control a robotic tadpole," in *2022 IEEE/RSJ International Conference on Intelligent Robots and Systems (IROS)*, pp. 6881–6887, IEEE, 2022.

[35] L. Li, L.-M. Chao, S. Wang, O. Deussen, and I. D. Couzin, "Robotwin: A platform to study hydrodynamic interactions in schooling fish," *IEEE Robotics & Automation Magazine*, 2024.